Journal of Power Sources 195 (2010) 1610–1614

Contents lists available at ScienceDirect

Journal of Power Sources

journal homepage: www.elsevier.com/locate/jpowsour

Short communication

# Design and preparation of highly active carbon nanotube-supported sulfated $TiO_2$ and platinum catalysts for methanol electrooxidation

Huanqiao Song, Pu Xiao, Xinping Qiu*, Wentao Zhu

*Key Laboratory of Organic Optoelectronics and Molecular Engineering, Department of Chemistry, Tsinghua University, Beijing 100084, China*

ARTICLE INFO

*Article history:*
Received 25 July 2009
Received in revised form
16 September 2009
Accepted 17 September 2009
Available online 26 September 2009

*Keywords:*
Electrocatalyst
Carbon nanotube
Structural design
High catalytic activity
CO tolerance
Direct methanol fuel cell

ABSTRACT

A novel electrocatalyst structure of carbon nanotube-supported sulfated $TiO_2$ and Pt (Pt–S–$TiO_2$/CNT) is reported. The Pt–S–$TiO_2$/CNT catalysts are prepared by a combination of improved sol–gel and ethylene glycol reduction methods. Transmission electron microscopy and X-ray diffraction show that the sulfated $TiO_2$ is amorphous and is coated uniformly on the surface of the CNTs. Pt nanoparticles of about 3.6 nm in size are homogenously dispersed on the sulfated $TiO_2$ surface. Fourier transform infrared spectroscopy analysis proves that the CNT surfaces are modified with sulfated $TiO_2$ and a high concentration of $SO_x$, and adsorbed OH species exist on the surface of the sulfated $TiO_2$. Electrochemical studies are carried out using chronoamperometry, cyclic voltammetry, CO stripping voltammetry and impedance spectroscopy. The results indicate that Pt–S–$TiO_2$/CNT catalysts have much higher catalytic activity and CO tolerance for methanol electrooxidation than Pt/$TiO_2$/CNTs, Pt/CNTs and commercial Pt/C.



## 1. Introduction

The direct methanol fuel cell (DMFC) is commonly considered as a candidate for future energy-generating devices because of its simple structure, liquid fuel and environmental cleanliness [1,2]. However, the performance of DMFCs is greatly hampered by the slow oxidation rate of methanol. It is generally accepted that poisoning of the Pt surface by CO-like species produced during methanol oxidation is the major reason for the low rate of reaction. To solve this problem, Pt-based alloys (including PtRu and PtSn) [3–5] and Pt/metal oxide composites (including Pt/$SnO_2$ and Pt/$RuO_2$) [6–8] have been used to increase the activity and CO tolerance of the catalysts, based on a bifunctional mechanism [9] or an electronic effect [10].

Recently, researchers have reported that systems combining platinum, metal oxides and carbon exhibited excellent catalytic activity for electrooxidation of methanol and CO. Justin and Ranga Rao [11] studied the electrochemical activity of Pt–$V_2O_5$/C catalysts for the oxidation of methanol and CO. The results indicated that Pt–$V_2O_5$/C composites performed better than a Pt/C catalyst. Avaca and colleagues [12] found that Pt–$RuO_2$/C composites prepared by the sol–gel technique showed a higher current density and better stability towards the oxidation of methanol compared with a commercial Pt/C powder. The large anodic current density and stability of the catalyst were considered to be the main reasons for the increased activity of the resulting electrode. Ha and colleagues [13] reported that Pt–$CeO_2$/C catalysts displayed a better activity towards the oxidation of methanol than unmodified Pt/C catalysts. The influence of ceria on the activity of the platinum catalyst was ascribed to both bifunctional and intrinsic mechanisms.

Pt, $TiO_2$ and carbon nanotube (CNT) composites, which are used as catalysts in the fields of sensors [14,15] and photoelectrochemical cells [16], have also exhibited excellent catalytic activity for the electrooxidation of methanol. Cai and colleagues [17] synthesized a $TiO_2$\CNT\Pt electrode by electrodepositing Pt nanoparticles on CNT-modified $TiO_2$. The $TiO_2$\CNT\Pt electrode displayed a higher and more stable electrocatalytic activity for methanol oxidation compared with a graphite\CNT\Pt electrode. In a previous study, we studied a Pt–$TiO_2$/CNT catalyst prepared by sol–gel and ethylene glycol reduction methods and found that a thin $TiO_2$ layer (<5 nm) acted as an efficient co-catalyst with Pt for ethanol electrooxidation [18]. However, a thicker $TiO_2$ layer (>5 nm) or larger particle size adsorbed on the carbon nanotubes could seriously affect the catalytic activity of the sample by decreasing the conductivity. A new co-catalyst is required that not only can improve the catalytic activity and CO tolerance of Pt, but also has high electron and proton conductivities.

Solid superacids, such as $SO_4^{2-}$–$ZrO_2$, $SO_4^{2-}$–$TiO_2$ and $SO_4^{2-}$–$Fe_2O_3$, are useful acid catalysts in selective hydrocarbon isomerization, acylation and esterification reactions due to their

* Corresponding author. Tel.: +86 10 62794234; fax: +86 10 62794234.
*E-mail address:* qiuxp@mail.tsinghua.edu.cn (X. Qiu).

0378-7753/$ – see front matter © 2009 Elsevier B.V. All rights reserved.
doi:10.1016/j.jpowsour.2009.09.045

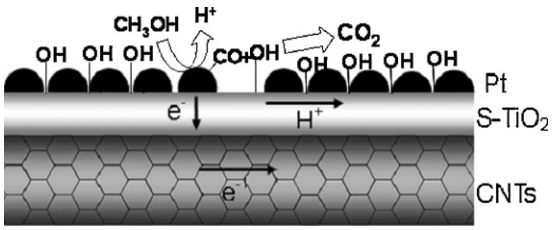


**Fig. 1.** Schematic diagram of the structure of the novel catalyst Pt–S–$TiO_2$/CNT.

strong Lewis acidity [19,20]. In addition, solid superacids show high proton conductivity because of their excellent hydrophilic properties. Guo et al. reported that a Pt–S–$ZrO_2$/CNT catalyst showed high activity for the oxidation of methanol owing to the interaction between Pt and sulfated $ZrO_2$ [21]. Pt particles that were not in direct contact with $SO_4^{2-}$–$ZrO_2$ nanoparticles were still poisoned with CO-like species. In this work, we synthesized a new carbon nanotube-supported sulfated $TiO_2$ and Pt (Pt–S–$TiO_2$/CNT) catalyst by improved sol–gel and ethylene glycol reduction methods. Careful structural design allowed the Pt nanoparticles to homogeneously disperse on a sulfated $TiO_2$ layer, which means that all of the Pt nanoparticles could be in direct contact with sulfated $TiO_2$. This special catalyst structure (Fig. 1) and the high proton conductivity of sulfated $TiO_2$ increased the catalytic activity and CO tolerance of Pt for methanol electrooxidation.

## 2. Experimental

### 2.1. Preparation and characterization of catalysts

S–$TiO_2$/CNTs were prepared by an improved sol–gel method. Tetrabutyl titanate was dissolved in ethanol with agitation to form a 10% solution. This solution was slowly added dropwise into an acetic acid solution to form a sol, and then diluted to a 5% solution by addition of ethanol. CNTs were added to the diluted sol. After agitation for 20 min and sonication for 15 min, the sol was dried at 90 °C in an oil bath. The obtained solid was ground and then treated with 0.5 M $H_2SO_4$ solution for 30 min and dried at 100 °C for 12 h. The samples were calcined at 500 °C under flowing $N_2$ for 1 h to form the S–$TiO_2$/CNT composite. Pt–S–$TiO_2$/CNT catalysts were prepared by reduction of chloroplatinic acid with ethylene glycol on the S–$TiO_2$/CNTs. The content of sulfated $TiO_2$ in the S–$TiO_2$/CNTs was 40 wt%. For comparison, Pt–$TiO_2$/CNT catalysts were also prepared by the same process without adding $H_2SO_4$.

The morphology of the catalysts was investigated by transmission electron microscopy (TEM, JEM-1200EX) operated at 100 kV and high-resolution transmission electron microscopy (HRTEM, JEOL model JEM-2010) at 200 kV. X-ray diffraction (XRD) was performed on a Bruker powder diffraction system (model D8 Advanced) with a Cu Kα radiation source. The $2\theta$ angular regions between 20° and 90° were investigated at a scan rate of 6° $min^{-1}$ with a step of 0.02°. The Fourier transform infrared (FT-IR) spectra were recorded in the range of 4000–400 $cm^{-1}$ on an infrared spectrometer (GX FT-IR, PerkinElmer, CA, USA), equipped with a deuterated triglycine sulfate detector. The elemental composition of the catalysts was determined using an energy dispersive X-ray spectrometer (EDS OXFORD INCA 300).

### 2.2. Electrochemical measurements

Electrochemical measurements were carried out at 25 °C in a three-electrode cell using a PARSTAT 2273 potentiostat controlled by PowerSuite® software (Princeton Applied Research). The working electrode was prepared by dispersing 1 mg of catalyst in a 25 μL mixture of Nafion solution (20% Nafion and 80% ethylene glycol) and 65 μL deionized water, performing ultrasonication for 30 min and then placing the resulting suspension on a gold substrate (1 cm × 1 cm) using a micropipette, followed by drying at 80 °C for 1 h in air. Pt gauze and a saturated calomel electrode (SCE) were used as the counter and reference electrodes, respectively. All potentials in this report are quoted versus SCE. Cyclic voltammetry (CV) was conducted at a rate of 50 mV $s^{-1}$ in a solution of 1 M $HClO_4$ or 1 M $CH_3OH$ + 1 M $HClO_4$, with potentials ranging from −0.2 to 1.0 V. Only the last cycle of 250 cycles was used for comparison of the catalytic activity of the specified catalysts. The chronoamperometric curves were recorded at 0.4 V for 3600 s and the electrochemical impedance spectroscopy (EIS) measurements were performed at a potential of 0.4 V in the frequency range between 100 kHz and 0.1 Hz. The oxidation of pre-adsorbed CO was measured by CO stripping voltammetry at a scan rate of 10 mV $s^{-1}$. The pH of all of the reaction solutions was 0.

## 3. Results and discussion

Fig. 2a and b show TEM images of the Pt–S–$TiO_2$/CNT catalysts. Fine Pt nanoparticles are homogeneously dispersed on the surface of S–$TiO_2$/CNTs without aggregation. The particle size of Pt was estimated to be 3–5 nm. The hollow structure of the CNTs was not clearly visible indicating the sulfated $TiO_2$ coating was present on the CNTs. EDS results confirm the presence of sulfated $TiO_2$ and the correct stoichiometry of the Pt–S–$TiO_2$/CNT composites. Fig. 3 displays the XRD patterns of the Pt–$TiO_2$/CNT and Pt–S–$TiO_2$/CNT composites. Two phases were identified in both patterns. One phase

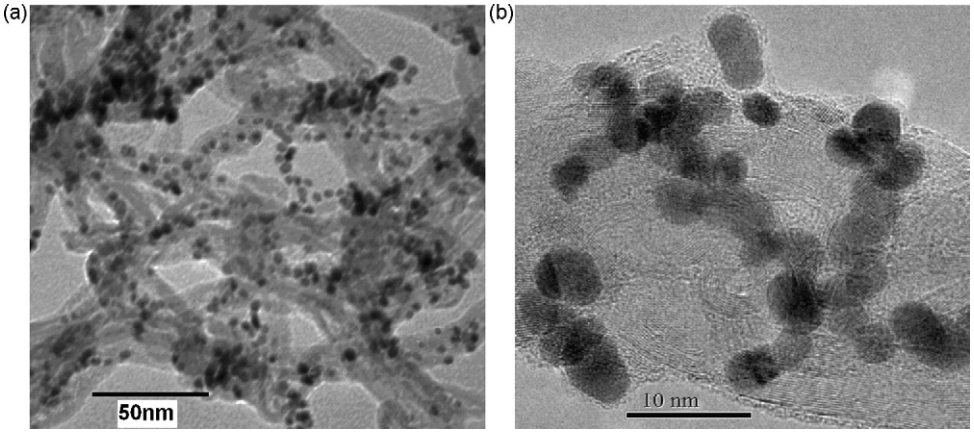


**Fig. 2.** (a) TEM and (b) HRTEM images of the Pt–S–$TiO_2$/CNT catalyst.

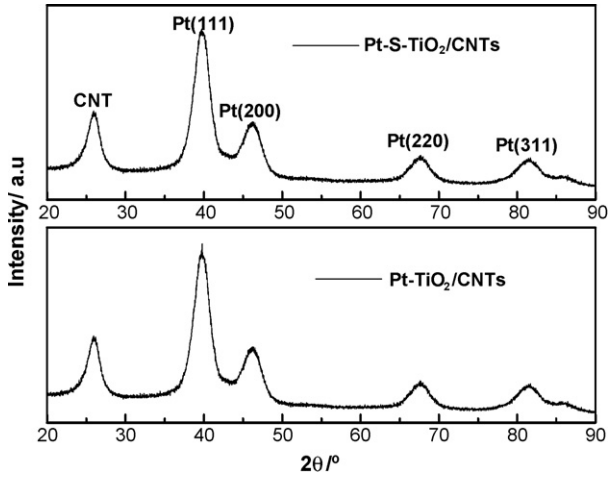


**Fig. 3.** XRD patterns of Pt–S–$TiO_2$/CNT and Pt–$TiO_2$/CNT.

was identified by the presence of peaks characteristic of crystalline face-centered cubic platinum (consistent with the (1 1 1), (2 0 0), (2 2 0) and (3 1 1) planes). The other phase showed a diffraction peak at around 26.0°, which is related to the crystalline nature of the graphitic structure of the CNTs. No peak was observed for $TiO_2$. This means that the as-prepared sulfated $TiO_2$ and the $TiO_2$ on CNTs were amorphous, which agrees well with our previous results [18]. No shifts were observed in the platinum peaks indicating that the sulfated $TiO_2$ additive has no effect on the crystal lattice of platinum. The average crystallite size of platinum calculated from the Pt (2 2 0) plane using the Scherrer formula was 3.6 nm for Pt–S–$TiO_2$/CNTs and 3.8 nm for Pt–$TiO_2$/CNTs, which is consistent with TEM observations. The FT-IR spectra of the S–$TiO_2$/CNTs and $TiO_2$/CNTs are presented in Fig. 4. Several absorption peaks in the 900–1300 $cm^{-1}$ region were observed in the spectra of the S–$TiO_2$/CNTs that were absent in the spectrum of the $TiO_2$/CNTs. These characteristic absorption peaks were consistent with S═O or S—O bonds, which implies the presence of a high concentration of $SO_x$ bonded tightly with Ti that could lead to high proton conductivity. The absorption peak at 1557 $cm^{-1}$ is characteristic of dissociative hydroxyls (OH) of $H_2O$ adsorbed on the S–$TiO_2$/CNTs. These hydroxyls are favorable for the oxidation of CO-like species [22].

The catalytic activities and stability of Pt–S–$TiO_2$/CNT and Pt–$TiO_2$/CNT catalysts for methanol oxidation have been investi-

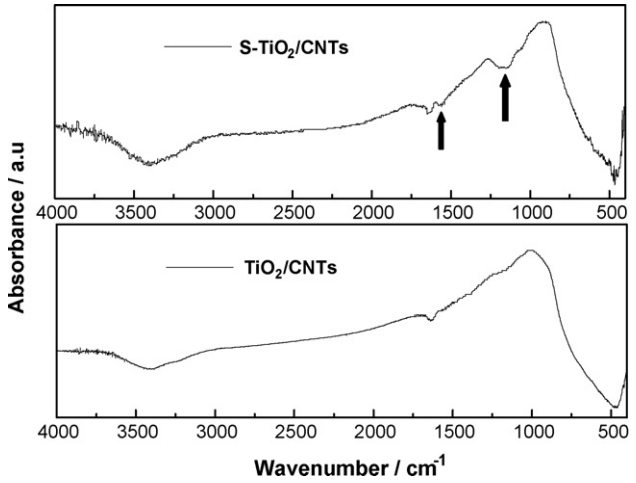


**Fig. 4.** FT-IR spectra of S–$TiO_2$/CNT and $TiO_2$/CNT.

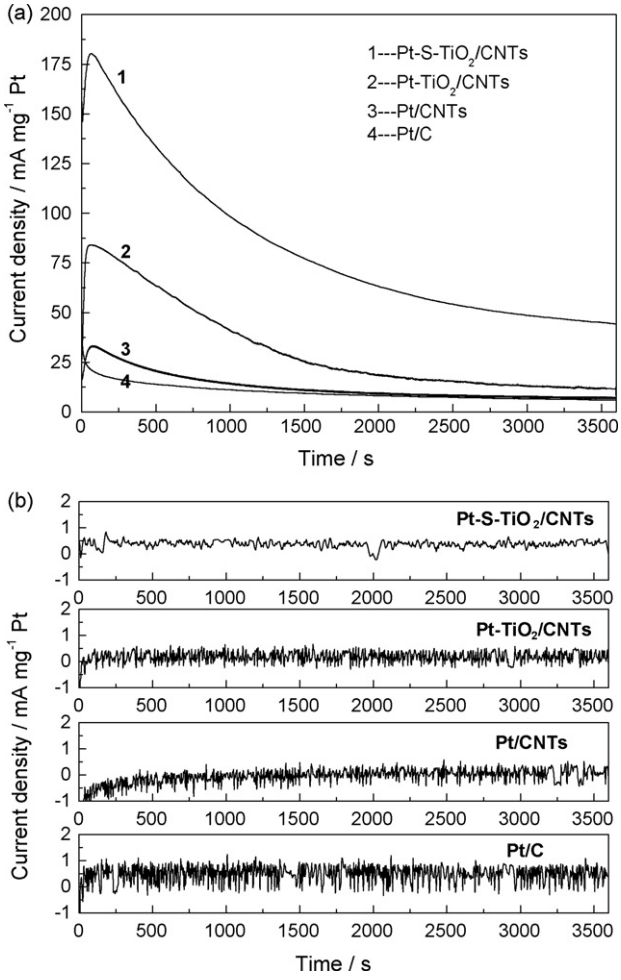


**Fig. 5.** Chronoamperograms recorded at 0.4 V for 3600 s at Pt–S–$TiO_2$/CNT, Pt–$TiO_2$/CNT, Pt/CNT and Pt/C electrodes: (a) in a solution containing 1 M $CH_3OH$ and 1 M $HClO_4$; (b) in a solution of 1 M $HClO_4$.

gated by chronoamperometric tests and the corresponding curves are shown in Fig. 5a. The current density–time curves of the Pt/CNTs and commercial Pt/C (20 wt% Pt, E-TEK) are also presented for comparison. As shown, at 0.4 V the initial current densities of the Pt–S–$TiO_2$/CNTs were significantly higher than those of the Pt–$TiO_2$/CNT catalysts although they both were much higher than those of the Pt/CNT and Pt/C catalysts. The current decayed more slowly for the Pt–S–$TiO_2$/CNTs than the Pt–$TiO_2$/CNTs indicating less accumulation of adsorbed CO species. The current densities decreased and then stabilized over the experimental period. At the end of the experimental period, the current density of the Pt–S–$TiO_2$/CNTs (46 mA $mg^{-1}$ Pt) was three and a half times higher than that of the Pt–$TiO_2$/CNT catalyst (13 mA $mg^{-1}$ Pt). This implies that the Pt–S–$TiO_2$/CNT composite exhibits higher catalytic activity and better stability than the Pt–$TiO_2$/CNT composite. The CV curves shown in Fig. 6 are also consistent with this finding. The onset potential (in the scan in the positive direction) of methanol oxidation on the Pt–S–$TiO_2$/CNTs was 0.28 V, which is much lower than the Pt–$TiO_2$/CNT (0.52 V), Pt/CNT (0.54 V) and Pt/C (0.48 V) catalysts. The maximum current densities (in the scan in the positive direction) of methanol oxidation were 536 mA $mg^{-1}$ Pt, 379 mA $mg^{-1}$ Pt, 341 mA $mg^{-1}$ Pt and 329 mA $mg^{-1}$ Pt for the Pt–S–$TiO_2$/CNTs, Pt–$TiO_2$/CNTs, Pt/CNTs and Pt/C, respectively. The lower onset potential and higher peak current density indicate that oxidation of methanol is more stable and more facile on the Pt–S–$TiO_2$/CNT electrode. Both the chronoamperometry and

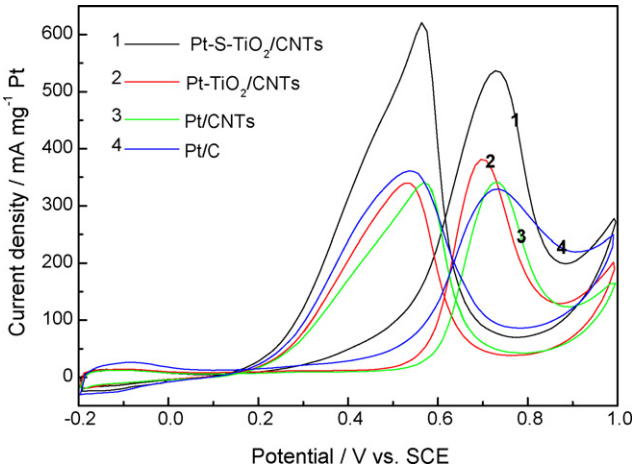


**Fig. 6.** Cyclic voltammograms recorded at Pt–S–$TiO_2$/CNT, Pt–$TiO_2$/CNT, Pt/CNT and Pt/C electrodes in a solution containing 1 M $HClO_4$ and 1 M $CH_3OH$ measured at a scan rate of 50 mV $s^{-1}$.

cyclic voltammetric data show that the S–$TiO_2$/CNTs efficiently co-catalyze methanol oxidation with Pt in catalysts with carefully designed structures.

Fig. 7 shows the CV curves of the prepared and reference catalysts in a supporting electrolyte of 1 M $HClO_4$. Well-defined hydrogen adsorption–desorption peaks are observed in the potential region of −0.2 to 0.06 V. Electrochemical active surface (EAS) areas were obtained by measuring the charge of the hydrogen desorption peak after subtracting the charge from the double-layer region and with the assumption that a smooth Pt electrode gives a hydrogen adsorption charge of 210 μC $cm^{-2}$. The EAS area for the Pt–S–$TiO_2$/CNTs was 545 $cm^2$ $g^{-1}$, which is close to that of the Pt–$TiO_2$/CNTs (523 $cm^2$ $g^{-1}$), Pt/CNTs (521 $cm^2$ $g^{-1}$) and Pt/C (517 $cm^2$ $g^{-1}$). This suggests that the increased activity of the Pt–S–$TiO_2$/CNT catalyst is not caused by an increase in the catalytic area of Pt.

CO stripping voltammetry was performed to investigate the ability of the Pt–S–$TiO_2$/CNT, Pt–$TiO_2$/CNT, Pt/CNT and Pt/C electrodes to electrooxidize CO. Fig. 8 shows the CO stripping voltammograms of the catalysts. Large differences are observed in the onset potential and peak potential of CO oxidation. The onset potential for the Pt–S–$TiO_2$/CNTs was at 0.38 V, which was about 0.09 V lower than that measured on the Pt–$TiO_2$/CNT electrode, showing that the addition of sulfated $TiO_2$ is more beneficial for

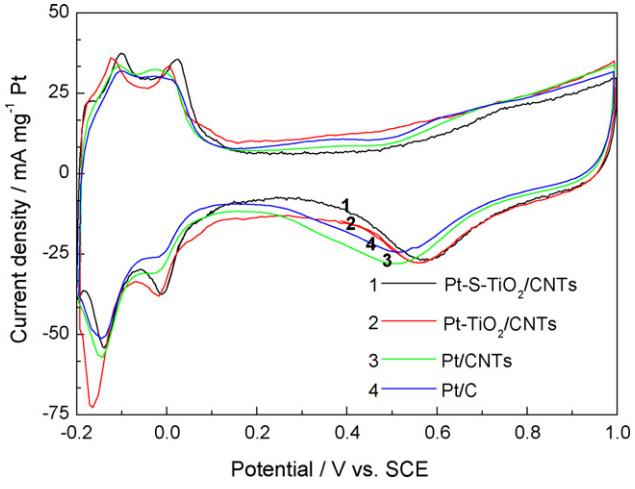


**Fig. 7.** Cyclic voltammograms recorded at Pt–S–$TiO_2$/CNT, Pt–$TiO_2$/CNT, Pt/CNT and Pt/C electrodes in 1 M $HClO_4$ solutions with a scan rate of 50 mV $s^{-1}$.

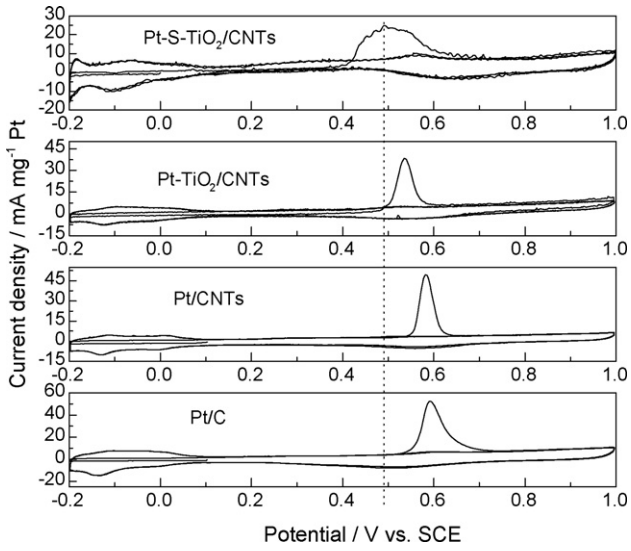


**Fig. 8.** CO stripping voltammograms recorded at Pt–S–$TiO_2$/CNT, Pt–$TiO_2$/CNT, Pt/CNT and Pt/C electrodes in 1 M $HClO_4$ solutions at a scan rate of 10 mV $s^{-1}$.

CO electrooxidation than the addition of $TiO_2$ alone. The highest onset potential (0.54 V) was found on the Pt/C electrode. The peak potentials of CO oxidation showed the same order as the onset potentials: Pt–S–$TiO_2$/CNT (0.49 V) < Pt–$TiO_2$/CNT (0.54 V) < Pt/CNT (0.58 V) < Pt/C (0.59 V). These results demonstrate that CO can be oxidized more quickly and readily on a Pt–S–$TiO_2$/CNT electrode than on Pt–$TiO_2$/CNT, Pt/CNT and Pt/C electrodes. This can be attributed to the presence of more absorbed OH ($OH_{ads}$) on the S–$TiO_2$/CNT electrode and the carefully designed structure of the Pt–S–$TiO_2$/CNT electrode. These two factors are favorable for a bifunctional mechanism.

EIS studies were carried out to reveal the intrinsic behavior of methanol electrooxidation by the catalysts. Fig. 9 shows the complex impedance plots for the Pt–S–$TiO_2$/CNT and Pt–$TiO_2$/CNT catalysts in solutions containing 1.0 M $CH_3OH$ and 1.0 M $HClO_4$. The Nyquist plots consist of left semicircle and right semicircle for each sample. The diameter of the right semicircle is a measure of the charge transfer resistance, which is related to the reaction kinetics of charge transfer [23]. The diameter of the right semicircle of Pt–S–$TiO_2$/CNTs is smaller than that of Pt–$TiO_2$/CNTs. Addition of sulfated $TiO_2$ to Pt/CNTs decreases the resistance to charge transfer more than $TiO_2$ alone does, indicating an improvement in the

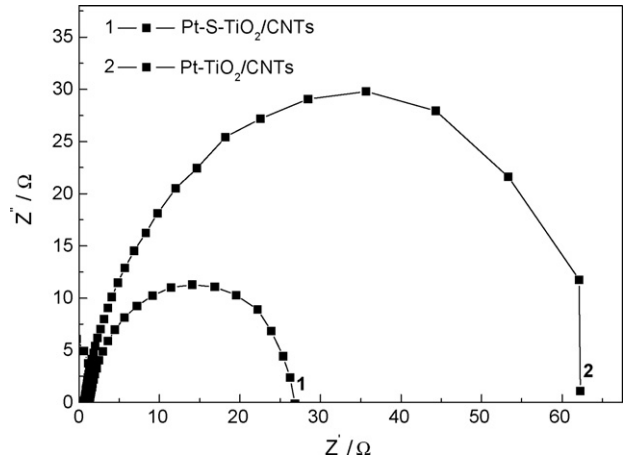


**Fig. 9.** Nyquist plots of impedance spectra recorded at Pt–S–$TiO_2$/CNT and Pt–$TiO_2$/CNT electrodes in a solution containing 1 M $CH_3OH$ and 1 M $HClO_4$ at 0.4 V.

kinetics of methanol oxidation using the Pt–S–$TiO_2$/CNT catalyst instead of the Pt–$TiO_2$/CNT one. This may be ascribed to the better electron and proton conductivity of the S–$TiO_2$/CNT support compared with the $TiO_2$/CNT support. Thus the Pt–S–$TiO_2$/CNT catalyst shows a higher catalytic activity for methanol oxidation than the Pt–$TiO_2$/CNT catalyst.

## 4. Conclusions

In this work, a new structurally controlled Pt–S–$TiO_2$/CNT catalyst was prepared using improved sol-gel and ethylene glycol reduction methods. TEM and XRD show that the Pt nanoparticles were uniformly adsorbed on the amorphous sulfated $TiO_2$-coated CNTs. FT-IR analysis indicated that $SO_x$ and $OH_{ads}$ also existed on the surface of the sulfated $TiO_2$. Electrochemical studies using chronoamperometry, cyclic voltammetry, CO stripping voltammetry and impedance spectroscopy found that the structure of the catalyst and a larger amount of $OH_{ads}$ increased the synergetic interaction between Pt and sulfated $TiO_2$. The high electron and proton conductivities of the Pt–S–$TiO_2$/CNT composite decreased the charge transfer resistance and increased the rate and current density of methanol oxidation. All these results reveal that the prepared catalyst is a promising anode catalyst for DMFC.

## Acknowledgment

This project was supported by the China Postdoctoral Science Foundation (project no. 20080440032).

## References

[1] Y. Chung, C. Pak, G.S. Park, W.S. Jeon, J.R. Kim, K. Lee, H. Chang, D. Seung, J. Phys. Chem. C 112 (2008) 313–318.
[2] A. Lam, D.P. Wilkinson, J.J. Zhang, Electrochem. Commun. 11 (2009) 1530–1534.
[3] C. Lim, R.G. Allen, K. Scott, J. Power Sources 161 (2006) 11–18.
[4] D.H. Lim, D.H. Choi, W.D. Lee, H.I. Lee, Appl. Catal. B: Environ. 89 (2009) 484–493.
[5] J.H. Choi, K.W. Park, I.S. Park, W.H. Nam, Y.E. Sung, Electrochim. Acta 50 (2004) 787–790.
[6] S. Jayaraman, T.F. Jaramillo, S.H. Baeck, E.W. Mcfarland, J. Phys. Chem. B 109 (2005) 22958–22966.
[7] A. Lan, A.S. Mukasyan, Ind. Eng. Chem. Res. 47 (2008) 8989–8994.
[8] L.P.R. Profeti, D. Profeti, P. Olivi, Int. J. Hydrogen Energy 34 (2009) 2747–2757.
[9] J.M. Léger, S. Rousseau, C. Coutanceau, F. Hahn, C. Lamy, Electrochim. Acta 50 (2005) 5118–5125.
[10] C. Lu, C. Rice, R.I. Masel, P.K. Babu, P. Waszczuk, H.S. Kim, E. Oldfield, A. Wieckowski, J. Phys. Chem. B 106 (2002) 9581–9589.
[11] P. Justin, G. Ranga Rao, Catal. Today 141 (2009) 138–143.
[12] H.B. Suffredini, V. Tricoli, N. Vatistas, L.A. Avaca, J. Power Sources 158 (2006) 124–128.
[13] M.A. Scibioh, S.K. Kim, E.A. Cho, T.H. Lim, S.A. Hong, H.Y. Ha, Appl. Catal. B: Environ. 84 (2008) 773–782.
[14] X.Y. Pang, D.M. He, S.L. Luo, Q.Y. Cai, Sens. Actuators B: Chem. 137 (2009) 134–138.
[15] K.N. Lin, W.J. Liou, T.Y. Yang, H.M. Lin, C.K. Lin, S.H. Chien, W.C. Chen, S.H. Wu, Diamond Relat. Mater. 18 (2009) 312–315.
[16] C.H. Kim, S.S. Hwang, J.H. Kim, K.H. Yoo, Curr. Appl. Phys. 10 (2010) 153–157.
[17] D.M. He, L.X. Yang, S.Y. Kuang, Q.Y. Cai, Electrochem. Commun. 9 (2007) 2467–2472.
[18] H.Q. Song, X.P. Qiu, F.S. Li, W.T. Zhu, L.Q. Chen, Electrochem. Commun. 9 (2007) 1416–1421.
[19] M. Busto, K. Shimizu, C.R. Vera, J.M. Grau, C.L. Pieck, M.A. D'Amato, M.T. Causa, M. Tovar, Appl. Catal. A: Gen. 348 (2008) 173–182.
[20] H.W. Chen, B. Wang, H.Z. Ma, X. Cui, J. Hazard. Mater. 150 (2008) 300–307.
[21] D.J. Guo, X.P. Qiu, W.T. Zhu, L.Q. Chen, Appl. Catal. B: Environ. 89 (2009) 597–601.
[22] A. Kabbabi, R. Faure, R. Durand, B. Bedan, F. Hahn, J.-M. Leger, C. Lamy, J. Electroanal. Chem. 444 (1998) 41–53.
[23] J. Otomo, X. Li, T. Kobayashi, C.J. Wen, H. Nagamoto, H. Takahashi, J. Electroanal. Chem. 573 (2004) 99–109.